A Computational Investigation of Side-by-Side Rotors in Ground Effect

Richard Healy PhD Student
Joseph McCauley Masters Student
Farhan Gandhi Redfern Professor
Onkar Sahni Associate Professor
Center for Mobility with Vertical Lift (MOVE), Rensselaer Polytechnic Institute, New York, USA

ABSTRACT

This study investigates the interactional aerodynamics of hovering side-by-side rotors in ground effect. The 5.5 ft diameter, 3-bladed fixed-pitched rotors are simulated using CFD at a targeted 5 lb/ft^2 disk loading. Simulations are performed using the commercial Navier Stokes solver, AcuSolve, with a detached eddy simulation (DES) model. Side-by-side rotors are simulated at two heights above the ground (H/D = 0.5 and H/D = 1), and with two hub-hub separation distances (3R and 2.5R). The performance of side-by-side rotors in ground effect are compared to isolated rotors out of ground effect. Between the side-by-side rotors in ground effect, a highly turbulent mixing region is identified where the wakes of each rotor collide. The flow fountains upwards, as well as exits outwards (along a direction normal to a plane connecting the two rotor hubs). The fountaining between rotors reaches up to 1.5R above the ground, and as blades at H/D = 0.5 traverse the highly turbulent flow, strong vibratory loading is induced, and a larger thrust loss is observed outboard between the rotors. Side-by-side rotors at H/D = 0.5 with 2.5R hub-hub spacing produce peak-to-peak thrust oscillations up to 16% the steady thrust. Rotors positioned higher, at H/D = 1 are above the turbulent mixing flow, and produce significantly lower vibratory loads. The spacing between rotors at H/D = 0.5 and 3R hub-hub separation allows strong vortical structures to develop between the rotors which move from side-to-side over multiple revolutions. When the vorticity is positioned closer to one of the rotors, it produces a greater lift deficit over the outboard region and higher vibratory loading. For rotors closer together, at H/D = 0.5 and 2.5R separation, the vortical structures between rotors are constrained to a more concentrated area, and show less side-to-side drift.

INTRODUCTION

Over the last few years there has been a significant interest in large multi-rotor eVTOL aircraft for Urban Air Mobility. One of the challenges associated with the modeling, simulation and performance prediction of these aircraft is the complex interactional aerodynamic flow fields of multiple rotors operating in close proximity. Several recent studies have used high-fidelity computations to represent these flows (see for e.g., Refs. 1–8), resulting in good physical insights as well as an understanding of beneficial geometries/configurations. It should be noted, though, that the above multi-rotor eVTOL interactional aerodynamic studies have all been conducted out of ground effect. During take-off and landing operations around vertiports, however, these multi-copters will be close to the ground, and rotor-rotor-ground aerodynamic interactions can be expected to strongly influence the performance and loads.

Although the understanding of rotors in ground effect is not new, the majority of prior studies in this area have focused on conventional single main rotor aircraft, or an isolated rotor in proximity of the ground. Early experiments by Fradenburgh (Ref. 9) identified performance improvements for rotors operating near the ground, and characterized how the wake moves radially outward after impacting the ground. Fradenburgh also identified flow inside the rotor wake moving upwards, towards the rotor disk. In recent studies, combinations of computational and experimental methods have been used to further understand ground effect aerodynamics. Using both experimental and computational fluid dynamics (CFD) simulation, Wadcock et. al. observed significant flow unsteadiness and upwash through the middle of the rotor disk due to ground effect on a UH-60 (Ref. 10). Kutz et. al. observed a 21% increase in thrust, as well as load oscillations when a Hughes 300C was simulated near the ground using CFD (Ref. 11). Lakshminarayan et. al. simulated a micro-scale rotor in ground effect and observed a thrust increase given constant power relative to when operating out of ground effect (Ref. 12). Flow unsteadiness was also observed below the rotor, which grew stronger as the rotor was brought closer to the ground. Experiments by Lee et. al. have characterized the aerodynamics of a rotor wake in ground effect using particle image velocimetry (Ref. 13).

Recent experimental and computational studies have investigated not only rotors in isolation, but also ones in close proximity to obstacles. A nearby wall can interfere with the nominally axisymmetric wake of an isolated rotor, and lead to rotor-obstacle interactional aerodynamic effects. Zanotti et. al. conducted experiments with a single rotor at a number of positions relative to a ground obstacle (Ref. 14). Ground effects when far from an obstacle were found to be significant

Presented at the Vertical Flight Society's 77th Annual Forum & Technology Display, Virtual, May 10-14, 2021.

at heights below three rotor radii. When the rotor was placed next to a vertical obstacle, reingestion effects were found to reduce rotor performance below that of a rotor out of ground effect. Viscous vortex partical method simulations matching Zanotti's experiments by Tan et. al. observed unsteady loads increasing as the rotor was brought laterally closer to the obstacle (Ref. 15). CFD simulations by Boisard observed reduced performance for a rotor located next to an obstacle as vertical distance to the ground was dropped (Ref. 16). Boisard also found that power was underestimated if the obstacle and ground were not fully modeled as no-slip.

While much of the existing literature on ground effect is for single main rotor helicopters, most large eVTOL vehicles employ multiple rotors for thrust generation and control. The aerodynamics of multiple close proximity rotors has been found to produce unique aerodynamic phenomena, particularly when operating near the ground. Actuator disk CFD simulations on a quad-tiltrotor by Gupta and Baeder showed highly complex flows between rotors when in close proximity to a ground plane (Ref. 17). Miesner et. al. simulated the eighteen rotor Volocopter 2x using CFD, and saw thrust fluctuations strengthen as rotors are brought closer to the ground (Ref. 18). Fluctuations were linked to mixing vortex structures between rotors which grew stronger close to the ground. Larger vortex structures were observed between rotors that were spaced farther apart.

The present work looks to use high fidelity blade resolved CFD to further investigate the aerodynamics of multiple close proximity rotors in ground effect. In particular, comparisons will be made between single rotors and side-by-side rotors in ground effect. Rotor to rotor spacing and height above the ground will be varied, and the aerodynamic interaction between rotors and the ground will be investigated. Physical explanations for differences in rotor performance between cases will also be provided.

ANALYSIS

Three single rotor and four side-by-side rotor cases are simulated using CFD. Single rotors are simulated in hover out of ground effect (OGE), at 0.5 rotor diameters above the ground (H/D = 0.5), and at 1 rotor diameter above the ground (H/D = 1) as shown in Fig. 1. Side-by-side rotors are also simulated in hover in ground effect (IGE) at H/D = 0.5 and H/D = 1, for two hub-to-hub separation values: 2.5R and 3R (also shown in Fig. 1). For the two rotor cases, the left rotor spins clockwise, and the right spins counterclockwise.

The rotors used have a $5.5ft$ diameter, with specifications detailed in Table 1, and are fitted with an idealized teardrop shaped hub to reduce the root wake and upwelling through the hub (Refs. 19, 20). The Rensselaer Multirotor Analysis Code (RMAC) (Ref. 21), based on blade element theory (BET) with 3x4 finite state Peters-He inflow representation is used to evaluate an appropriate root pitch and RPM for a target $5lb/ft^2$ disk loading in hover. A 22° root pitch, and 1600 revolutions per minute is found to provide sufficiently low power and hover tip Mach number. A low tip Mach number is desired to avoid compressibility effects and reduce noise. Rotor RPM is held constant for all cases while comparing rotor forces and moments in different configurations and conditions.

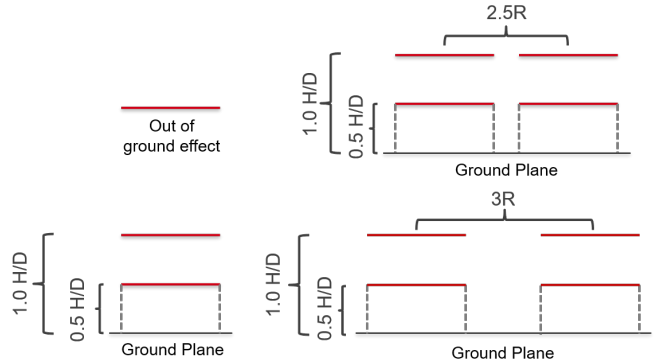

Figure 1. Simulation cases: 3 single rotor and 4 side-by-side

Table 1. Rotor Parameters

Parameter	Specification
Diameter	5.5 ft
Number of Blades	3
Solidity	0.076
Root Cutout	0.2R
Airfoil	NACA 23012
Twist	$-10°$ / span
Planform	Rectangular
Chord	3.28 in
Root Pitch	22°
RPM	1600 RPM

All simulations are conducted using the commercial Navier-Stokes solver AcuSolve which uses a stabilized 2nd order upwind finite element method, and is validated for external aerodynamic flows (Refs. 22, 23). AcuSolve simulations for an SUI Endurance rotor were previously shown to compare well against experimental results (Ref. 24). For a 2-rotor unit, the computational domain is shown in Fig. 2. The nonrotating volume is a rectangular prism with sides at least 25 rotor radii away from the front rotor hub. The sides and top boundaries are set to outflow with backflow conditions enabled, which allows for flow in either direction across the boundary with zero pressure offset. The bottom surface is set to no-slip condition in a weak fashion with a log-law based wall function (Ref. 25). The weak boundary condition acts like a wall model (Ref. 26) without the impractical computational cost associated with resolving the boundary layer on the ground. No-slip wall condition (enforced strongly or weakly) has been found to capture necessary viscous effects for accurately predicting rotor performance in ground effect (Ref. 16). Around each rotor is a cylindrical rotating volume with radius 1.06 rotor radii and extending two tip chord lengths above and below the extents of the rotor hub. Each surface of the cylindrical rotating volumes has a sliding mesh interface which passes information to and from the non-rotating volume that comprises the remainder of the computational domain.

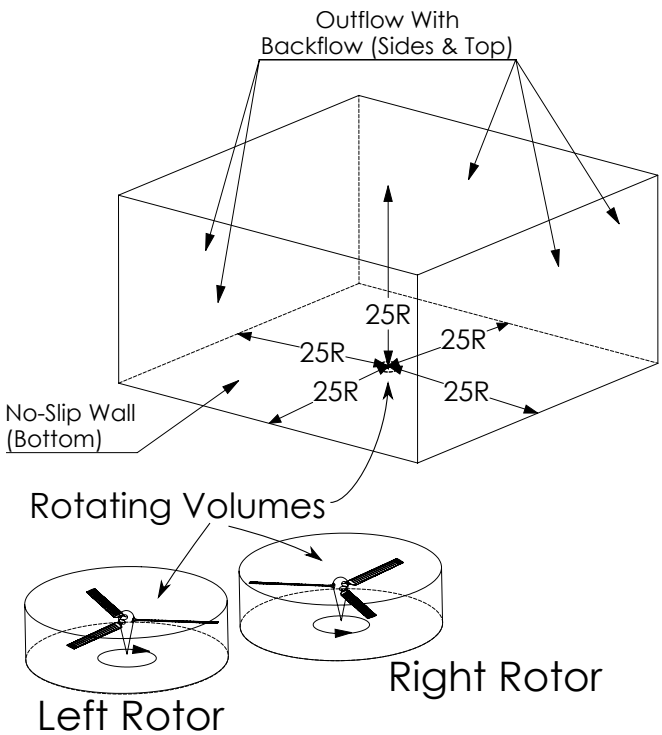

Figure 2. Diagram of the computational domain

The computational domain is discretized using an entirely unstructured mesh comprised of tetrahedral elements. On each blade, the surface mesh is set to ensure 200 elements around the airfoil countour, with refinement along the leading and trailing edges. The boundary layer in the wall-normal direction is highly resolved, with the first element height set to ensure a $y+ < 1$. The boundary layer is grown until the last layer size is within 80% of the local off-body element size (43 layers total). A portion of the blade surface mesh and a clipped slice of the boundary layer mesh is shown in Fig. 3. Around the rotors (1R above and below), a cylindrical wake refinement region is defined in which the element size is prescribed as $\frac{1}{4}$ blade chord (Fig. 4). Surrounding the first refinement region is a second refinement region which is prescribed with elements $\frac{1}{2}$ blade chord in size (Fig. 4). This refinement region extends radially from the bottom of each rotor hub, and grows wider near the ground. A third refinement region with 1 blade chord element size extends radially 10 rotor radii from each rotor hub (Fig. 4). A boundary layer mesh is grown off of the ground to capture the necessary viscous effects. While it is computationally too expensive to resolve the boundary layer with first layer height set to ensure $y+ < 1$, wall modeling allows for $y+ < 100$ to be acceptable. The entire computational domain is comprised of approximately 170 million elements for side-by-side cases, with 50 million in each rotating volume, and 70 million in the surrounding non-rotating volume. These rotor mesh parameters have been used in previously published AcuSolve rotorcraft simulations, and have been found to provide good spatial convergence (Refs. 3 and 4).

A detached eddy simulation (DES) is used with the Spalart-Allmarus (SA) turbulence model on-body for all simulations.

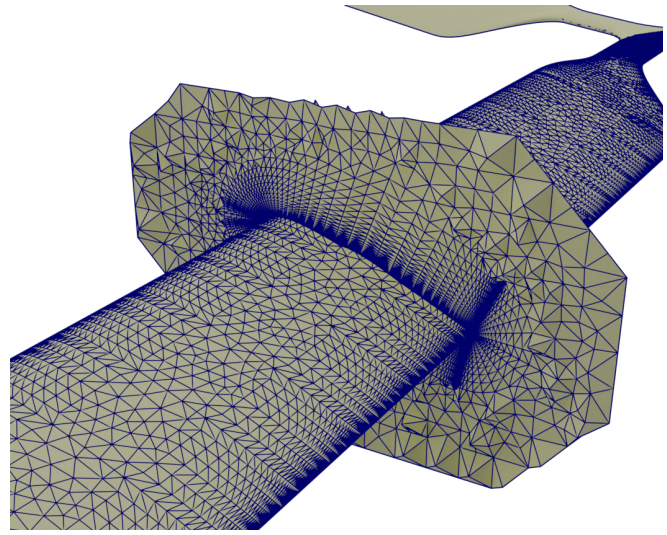

Figure 3. Blade surface mesh viewed near mid span, and a chordwise slice showing the boundary layer mesh in the wall-normal direction

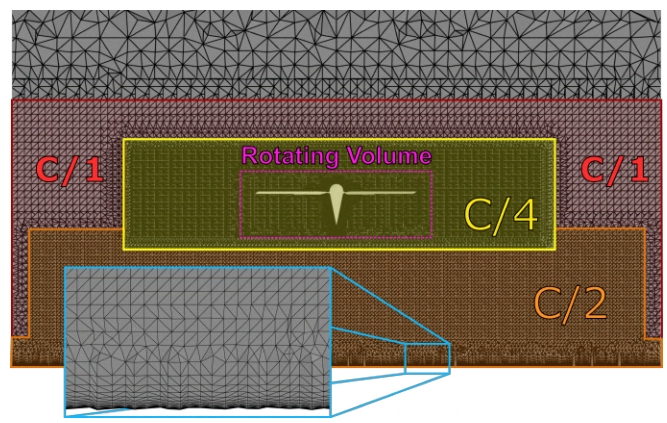

Figure 4. Cross-section of wake mesh refinement

Each case is initially run using time steps corresponding to 10° of rotation for at least 40 revolutions in order to reduce the computational cost of rotor wake development. These initial 10° time steps are possible without numerical divergence due to the stability afforded by the Streamline Upwind Petrov-Galerkin (SUPG) stabilized finite element method and generalized α implicit time integration method. The latter method was designed to suppress high frequency distrubances and allow solution stability with Courant-Friedrichs-Lewy (CFL) number greater than 1 (Refs 27, 28). Following the revolutions simulated with 10° time steps, an additional 5 revolutions (at minimum) are performed with time steps corresponding to 1°. Rotor forces and moments are averaged over the final three revolutions of the simulation. If average loads are not converged, additional revolutions are simulated. All runs are performed on 8 24 core AMD Epyc 7451 processors, part of the Center for Computational Innovations (CCI) at Rensselaer Polytechnic Institute. Wall time for the seven simulations in Fig. 1 totals over 2,200 hours (3 months).

RESULTS

Isolated Rotors in Ground Effect

A single hovering rotor in ground effect at H/D = 0.5 is simulated, and its performance is compared to a rotor hovering out of ground effect. Figure 5 shows the difference in sectional thrust coefficient between the two cases (IGE minus OGE). Here, red represents an increase in thrust compared to OGE, and blue represents a thrust deficit compared to OGE. Thrust increment is observed on the interior of the disk (from the root to 0.85R), whereas thrust deficit is observed near the tips. Overall, integrated rotor thrust IGE at H/D = 0.5 is 7% greater than OGE.

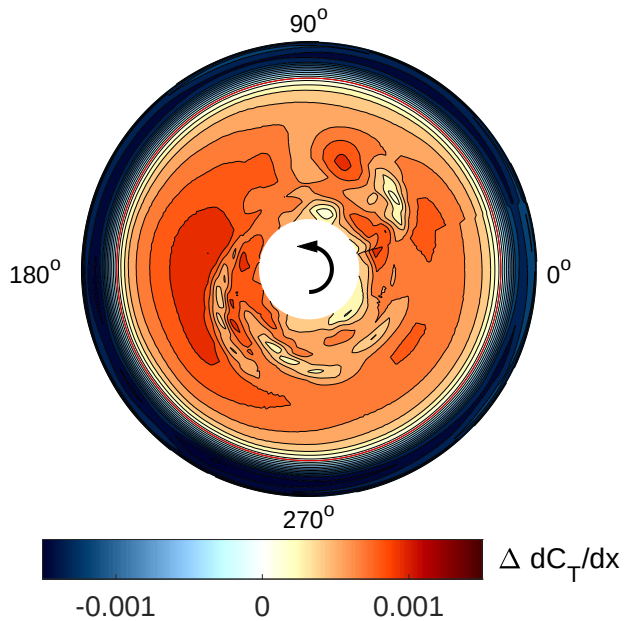

Figure 5. Sectional thrust coefficient difference between a single IGE rotor at H/D = 0.5, and an OGE rotor (IGE minus OGE)

The presence of a ground plane influences rotor performance by changing the wake aerodynamics. Figure 6 shows a slice through the hub colored by vertical velocity for OGE and IGE (H/D = 0.5) cases with velocity direction vectors. For the OGE case, the dark blue wake freely convects downwards. When the ground plane is introduced however, the wake impinges on the ground plane. Tip vortices of the wake impact the ground, and spread outward radially. Inside the wake, flow is constrained by both the ground plane, and the outboard wake. With nowhere to go, the inboard section of the flow fountains upwards around the hub region. Strong turbulence is observed within the fountaining region with many vortical structures mixing and interacting.

The relationship between wake structure and thrust production can be seen by looking at vertical velocity over the rotor disk. Figure 7 shows vertical velocity at the rotor plane for OGE and IGE (H/D = 0.5) rotors. The vertical velocity difference between the cases (IGE minus OGE) is also shown. On the inboard sections of the blade, a positive difference in velocity is observed. With the two left vertical velocity plots showing downward velocity (blue) in this region, this indicates a reduction in downwash induced by the IGE rotor (compared to the OGE rotor). Fountaining on the inboard regions of the rotor induces relative upwash on the inboard blade sections. Upwash on inboard blade sections leads to increase in angle of attack and the the relative increase in thrust observed in Fig. 5. The IGE rotor shows a thrust deficit over the tip region (see dark blue peripheral ring at radial stations outboard of 85% in Fig. 5). This is a result of higher downwash at the blade tips (see dark purple region on the right slice of Fig. 7 and can be attributed to the recirculating flow in ground effect.

An isolated rotor in ground effect at H/D = 1 is also simulated. Figure 8 shows a slice through the hub colored by vertical velocity for IGE (H/D = 1) and IGE (H/D = 0.5) cases. Like with the rotor at H/D = 0.5, the wake generated by a rotor IGE at H/D = 1 convects downwards until it hits the ground plane, and proceeds to spread radially. Flow on the inboard portion of the wake is still trapped, leading to strong turbulence, but is too far below the rotor to fountain through the disk plane.

Without the flow fountaining through the central region of the rotor disk, the thrust distribution of the rotor at H/D = 1 is different than that at H/D = 0.5. Figure 9 shows the sectional thrust coefficient difference between a rotor IGE (H/D = 1) and a rotor OGE (IGE minus OGE). Without fountaining reaching the disk plane, the IGE rotor at H/D = 1 does not show any thrust increment on the inboard sections. Like the isolated IGE rotor at H/D = 0.5, moderate thrust deficit is observed near the blade tips due to recirculating flow, but this too is weaker than the H/D = 0.5 case in Fig. 5. Overall, only a 1% decrease in thrust is observed for the H/D = 1 rotor compared to OGE.

Side by Side H/D = 0.5

Simulation of side-by-side rotors at H/D = 0.5 and 3.0R hub-hub separation is presented next. Figure 10 shows a direct volume rendering of vorticity magnitude for side-by-side rotors at 3R separation. Portions of the flow field with greater vorticity magnitude are rendered with greater opacity. Tip paths for each rotor are annotated as cyan rings. A cyan grid is also plotted parallel to the $\psi = 90^\circ - 270^\circ$ line between the rotors which extends from the ground plane to 1R above the rotor plane. From $\psi = 270^\circ$ to 90° (through 0° in the direction of rotation), the right rotor wake has a similar structure to that of a single rotor. Tip vortices convect down and impact the ground, then move radially away from the rotor. On the side of the disk facing the other rotor however, the flow from the two rotors collide and the flow is constrained from moving radially. Where the wakes collide, mixing produces a wall of strong turbulence between the rotors, in the inter-rotor region. This wall extends upwards and outwards and intersects the tip-path-plane of the rotors (covering both the cyan tip path plane rings and the middle cyan grid).

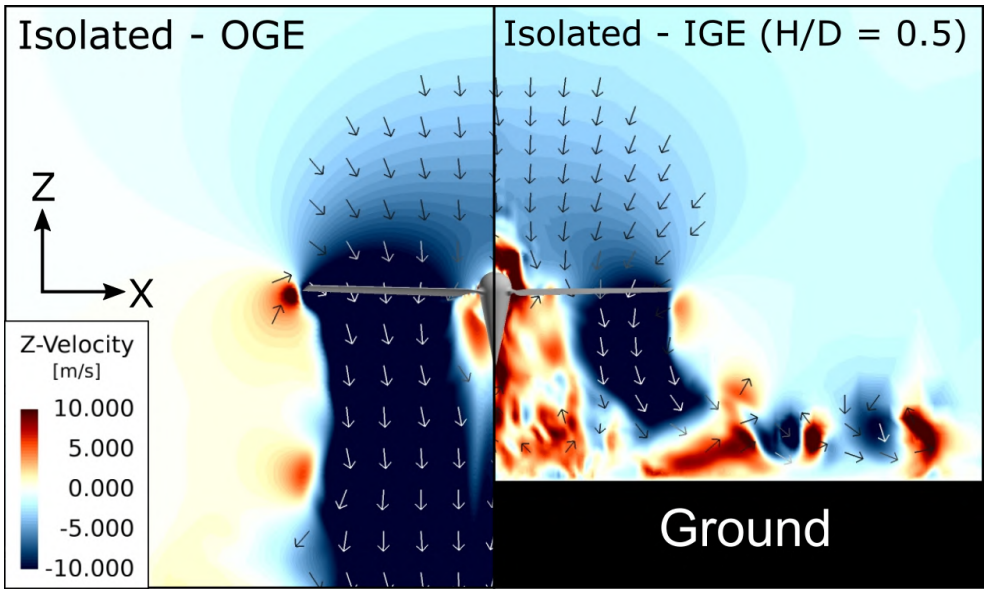

Figure 6. Slice colored by vertical velocity for OGE and IGE (H= 0.5) rotors

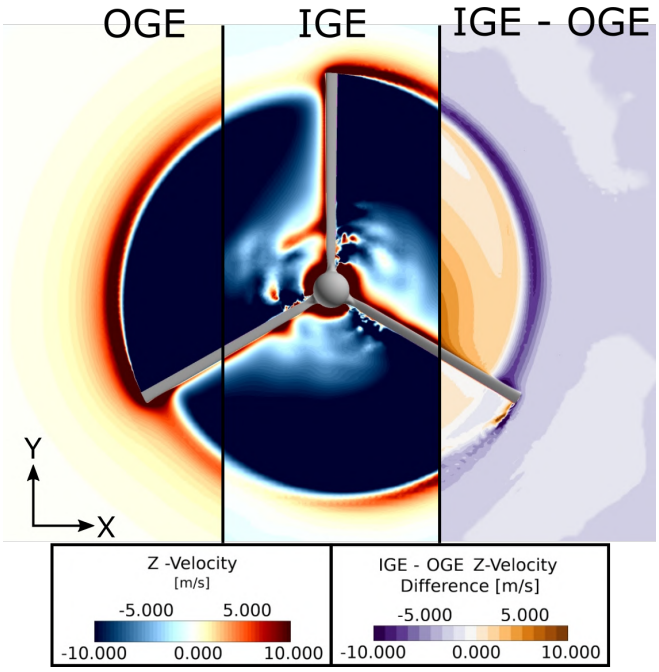

Figure 7. Vertical velocity through OGE and IGE (H/D = 0.5) rotor disks, as well as vertical velocity difference (IGE minus OGE) at the rotor plane

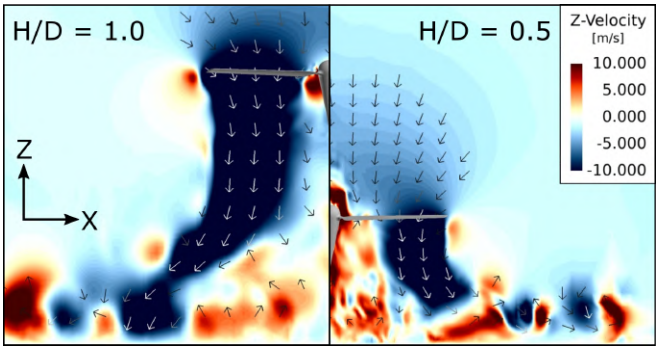

Figure 8. Slice cutting through the hub of H/D = 1 IGE and H/D = 0.5 IGE rotor hubs colored by vertical velocity

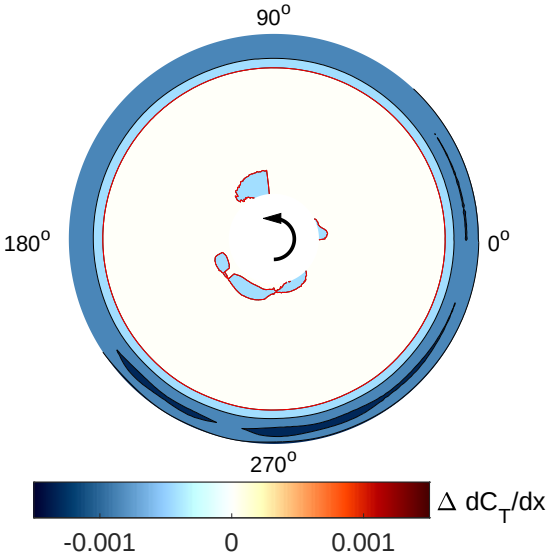

Figure 9. Sectional thrust coefficient difference between a single rotor IGE rotor at H/D = 1, and an OGE rotor (IGE minus OGE)

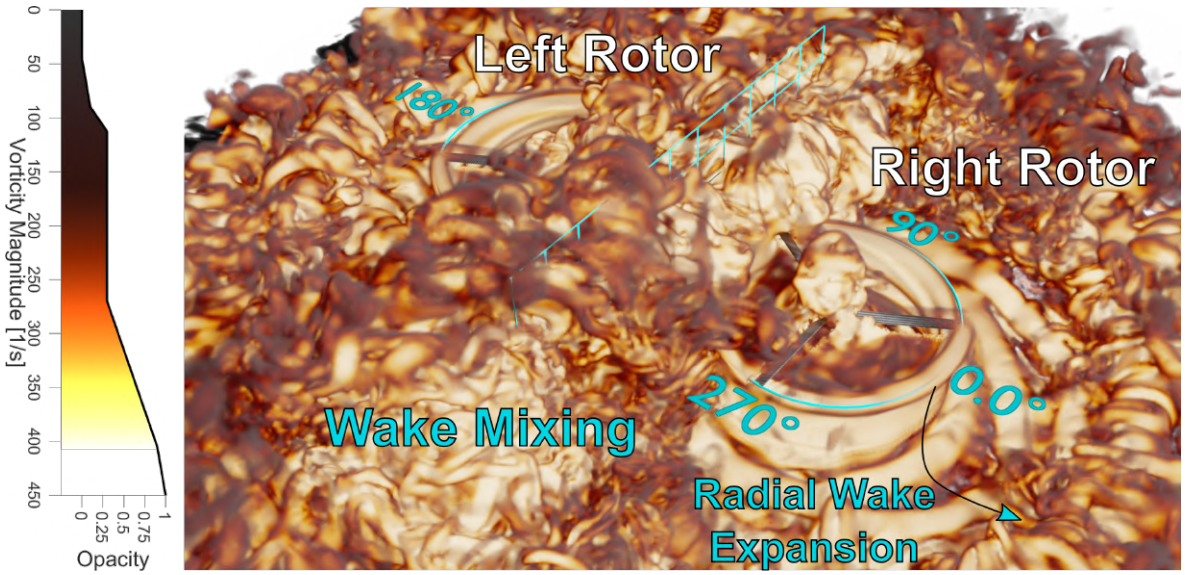

Figure 10. Direct volume rendering of H/D = 0.5, 3.0R separation side-by-side rotors with opacity and color dictated by vorticity magnitude

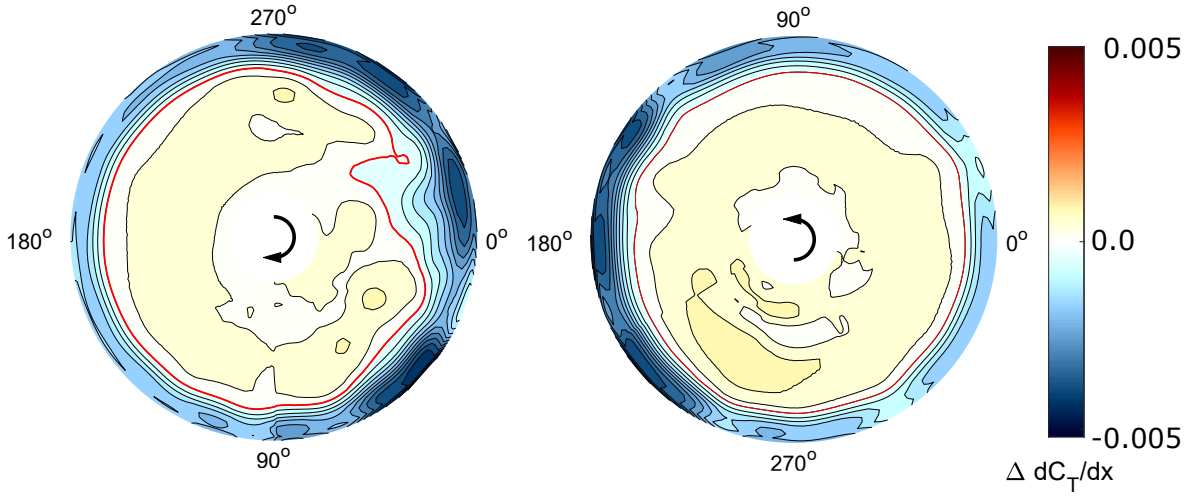

Figure 11. Three revolution average sectional thrust coefficient difference between side-by-side H/D = 0.5 rotors with 3.0R spacing and a single rotor out of ground effect rotor (IGE minus OGE)

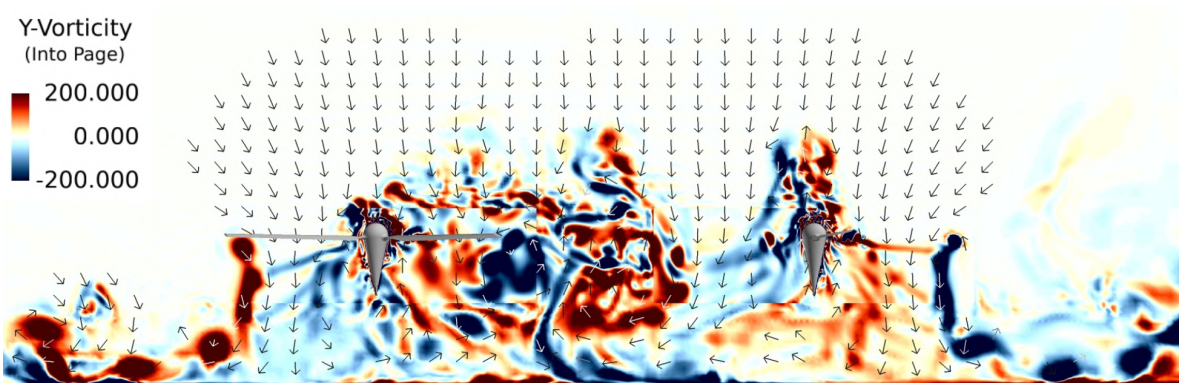

Figure 12. Slice cutting through side-by-side H/D = 0.5 3.0R separation IGE rotor hubs colored by Y-vorticity

Figure 11 shows the difference in sectional thrust coefficient between the two IGE rotors and an OGE single rotor (IGE minus OGE), phase averaged over three revolutions. Moderate thrust increment inboard, and thrust deficit outboard are observed like with the single rotor IGE case. However, with the presence of two rotors, larger thrust losses are observed at the tips when the blades pass between the rotors. The losses are also dissimilar in distribution between the rotors, and change from revolution to revolution due to the highly chaotic vortical flow in the inter-rotor region.

The unsteady thrust produced by side-by-side rotors in ground effect suggests interactional aerodynamics between the rotors. Figure 12 shows a slice cutting through both rotor hubs colored by vorticity in the +Y direction (into the page). Velocity direction vectors are also shown. On the outsides of the system, tip vortices are observed to move downwards and outward radially upon impacting the ground (similar to a single rotor IGE). Between the rotors however, substantial wake mixing is observed. The wakes of each rotor collide in the middle to produce a highly turbulent vortical flow with substantial mixing. As each blade passes through the inter-rotor region, it intersects with the vortical flow between the rotors. Tip vortices generated between the rotors are pulled into the mixing region, perpetuating the turbulent nature of the region. Turbulent mixing flow fountains above the rotors and intersects with the disk planes. As the blades pass through the turbulent mixing, impulsive loading is induced.

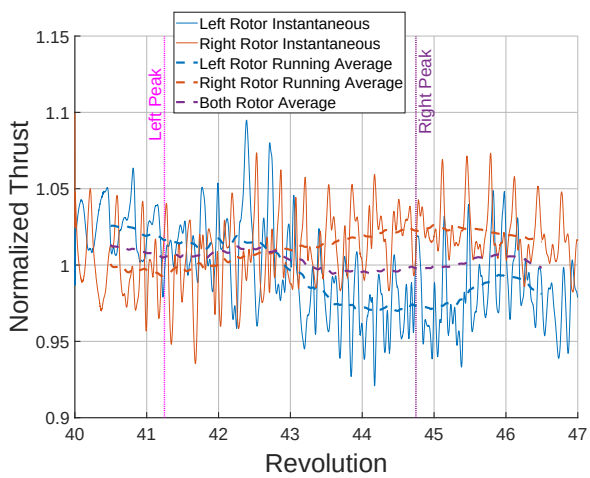

Figure 13. Thrust history of each side-by-side rotor at H/D = 0.5 and 3.0R hub-hub separation, including instantaneous, single rotor rev-averaged thrust and both rotor rev-averaged thrust normalized by isolated OGE rotor thrust

Figure 13 shows the thrust history for each side-by-side rotor at H/D = 0.5 and 3.0R separation normalized by isolated OGE rotor thrust. Running average thrust over one revolution is also presented for each rotor, as well as average thrust between the two rotors. Substantial vibratory loading is observed for both rotors as blades pass through the center mixing region. Average thrust over one revolution is not steady, with the left rotor average thrust changing by greater than 5% over the revolutions plotted (and the right rotor changing by 3%). The relative performance between rotors changes as well, with the left rotor producing more thrust at certain revolutions, and the right rotor producing more at others (depending on the predominant position of the unsteady vortical flow in the inter-rotor region). Average thrust of both rotors is relatively stable, only changing by approximately 2% over these seven revolutions. Overall, the thrust increment gained inboard is canceled by thrust deficits received between the rotors. Averaging over three revolutions at 1° timesteps, the side-by-side rotors at H/D = 0.5 with 3.0R spacing produce 0.2% less thrust than a single rotor OGE.

Changes in mean thrust from revolution to revolution are caused by pockets of strong vorticity moving within the mixing region at a rate slower than 1/rev. Figure 14 shows a slice cutting through both rotor hubs colored by vorticity magnitude with velocity streamlines. The top half corresponds to a time in the simulation when the left rotor produces more thrust (pink line in Fig. 13), and the bottom corresponds to when the right rotor produces more thrust (purple line in Fig. 13). When the left rotor is producing greater thrust, vortical mixing between the rotors has fountained up and over the right rotor, and the left rotor avoids the strongest turbulence. In contrast, when the right rotor is producing greater thrust, a majority of the vorticity is above the left rotor where it has a strong influence on left rotor performance.

The harmonic content of the blade loading depends on the relative position of the vortical mixing between the rotors. For example, between revolutions 45 and 46 in Fig. 13 when the right rotor is producing more thrust, most of the turbulent mixing is away from the right rotor (bottom of Fig. 14), and a predominantly 3/rev signal is observed. During the same time period however (between revolutions 45 and 46), the left rotor is subject to the mixing flow, and produces higher frequency thrust vibrations (Fig. 13). In general, when the vortical mixing is closer to a given rotor, it has a wider range of azimuths over which its blades will encounter turbulence and produces higher frequency harmonic loads. The strength of vibratory loading is notable as well. Peak-to-peak changes in instantaneous thrust can vary from 6% up to 10%.

Another side-by-side rotor system at H/D = 0.5 is also simulated with 2.5R rotor-rotor spacing. Figure 15 shows direct volume rendering of vorticity magnitude for side-by-side rotors with closer 2.5R spacing. Tip paths for each rotor are displayed as cyan rings. A cyan grid is also plotted parallel to the $\psi = 90° - 270°$ line between the rotors. Just as when the rotors had 3.0R hub-hub separation, the wake of the right rotor from $\psi = 270°$ to 90° behaves much the same way as the isolated H/D = 0.5 wake. However, between the rotors, wake mixing for the 2.5R separation case is weaker than with 3.0R separation, and occupies a lesser portion of the domain. Whereas mixing for the 3.0R separation case reaches above the top of the grid (1.0R above the rotor plane), the mixing with 2.5R separation only reaches one square above the disk plane (1/3R above). Strong vorticity also covers less of the tip path plane, indicating blades will encounter strong vorticity over a smaller range of azimuths.

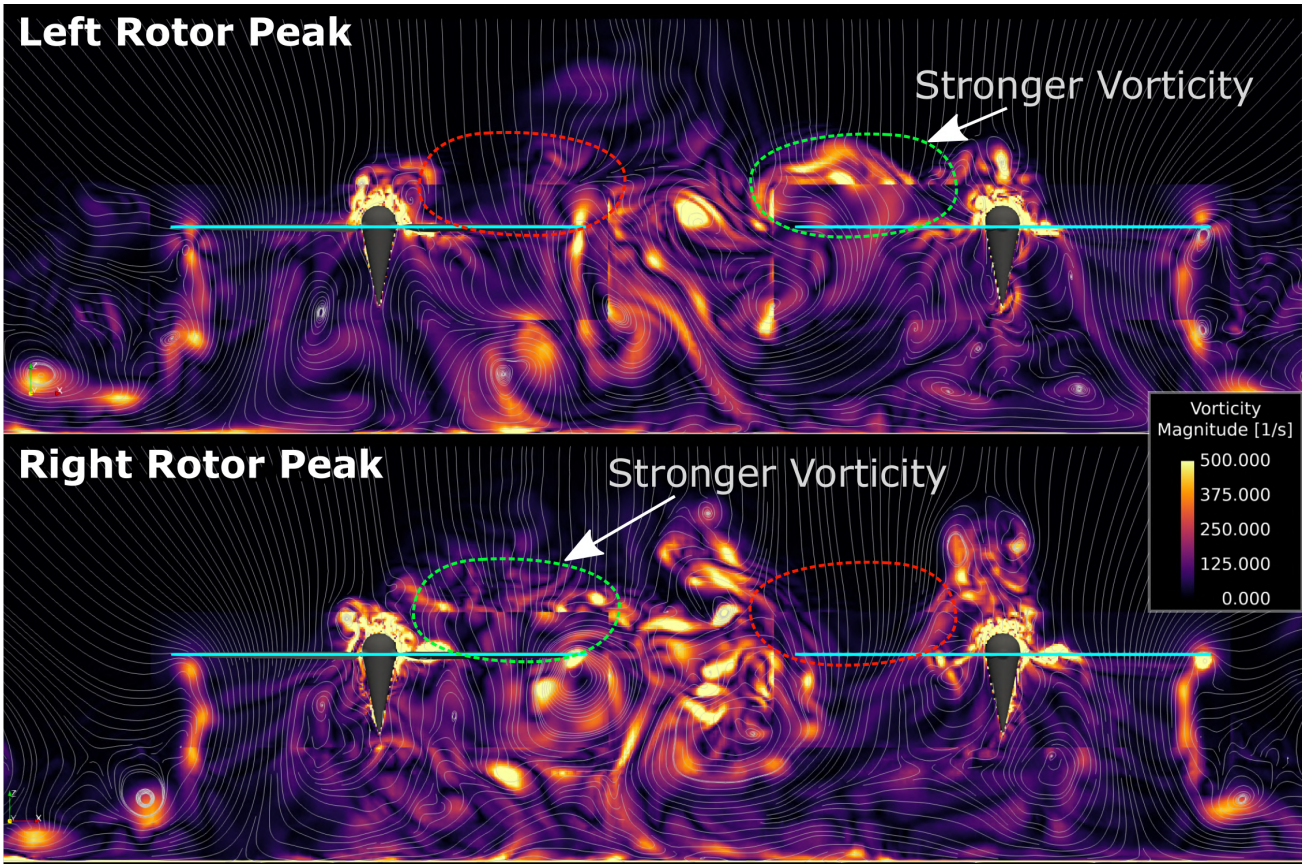

Figure 14. Slice cutting through side-by-side H/D = 0.5 3.0R separation IGE rotor hubs colored by vorticity magnitude at two different timesteps with white velocity streamlines

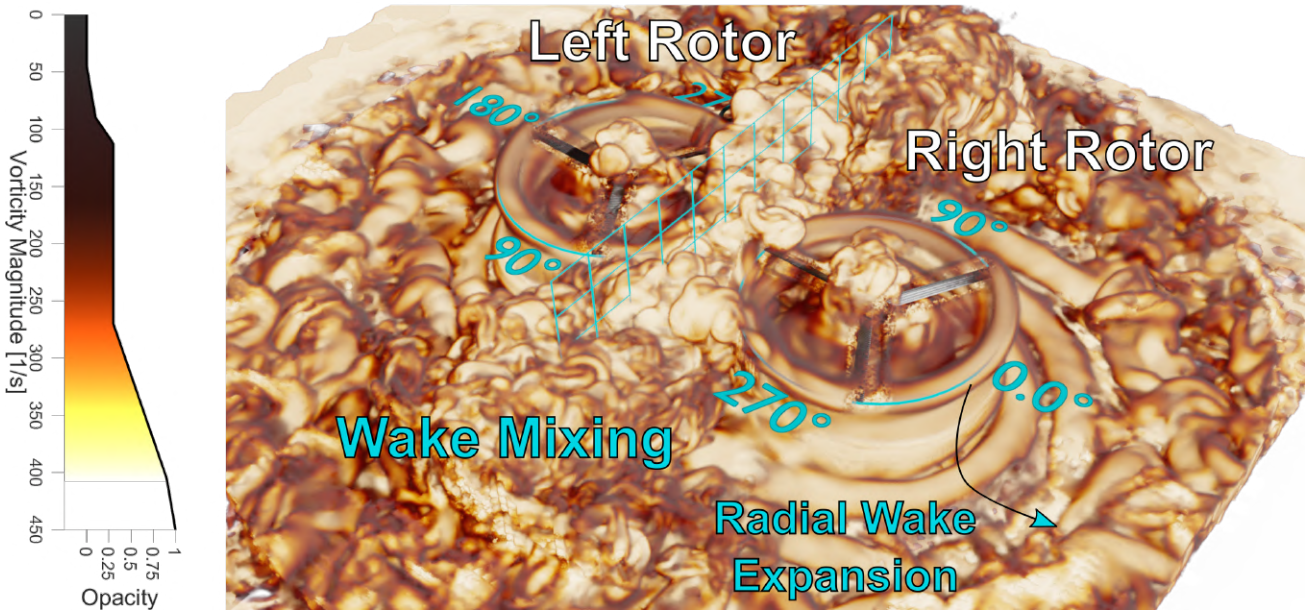

Figure 15. Direct volume rendering of side-by-side rotors at H/D = 0.5 and 2.5R separation with opacity and color dictated by vorticity magnitude

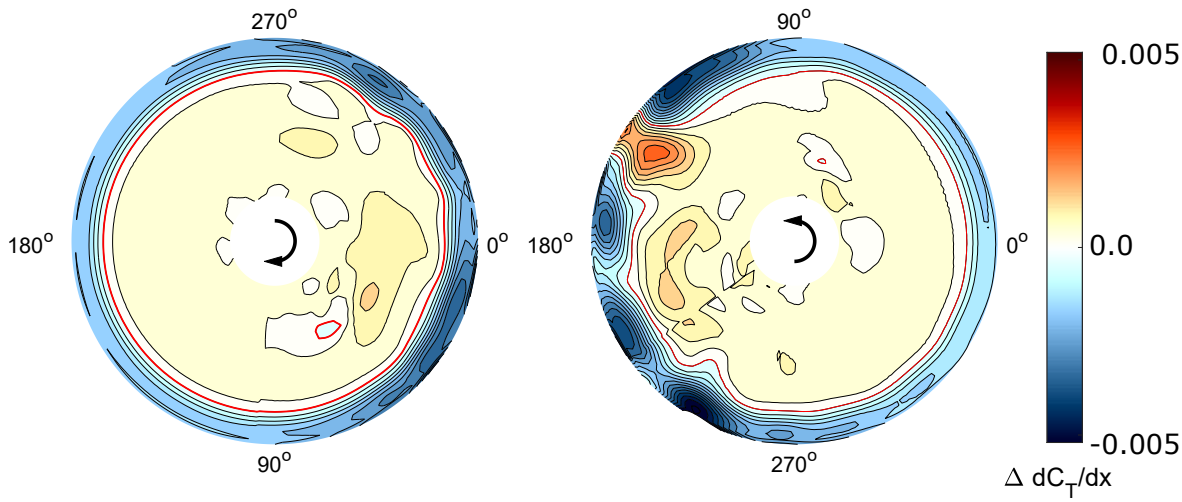

Figure 16. Three revolution average sectional thrust coefficient difference between side-by-side H/D = 0.5 rotors with 2.5R spacing and a single out of ground effect rotor

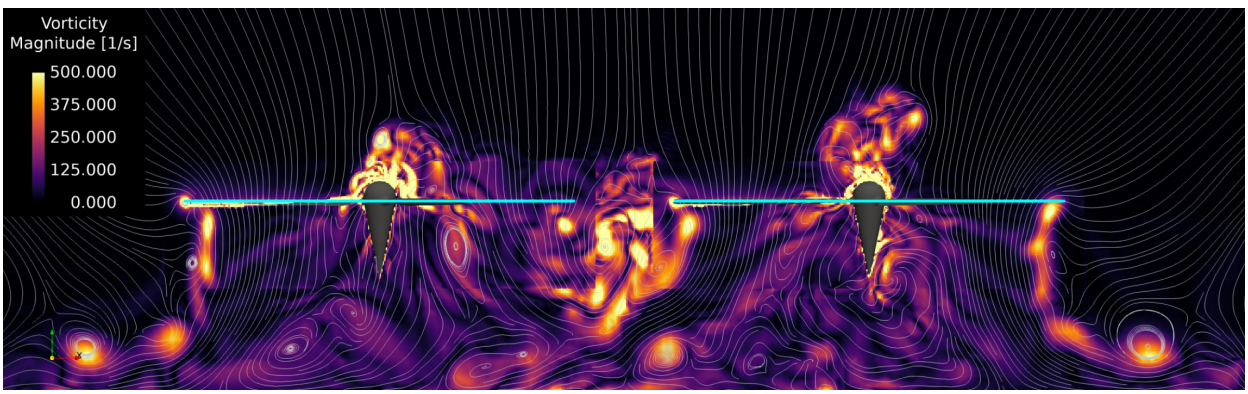

Figure 17. Slice cutting through side-by-side H/D = 0.5 2.5R separation IGE rotor hubs colored by vorticity magnitude

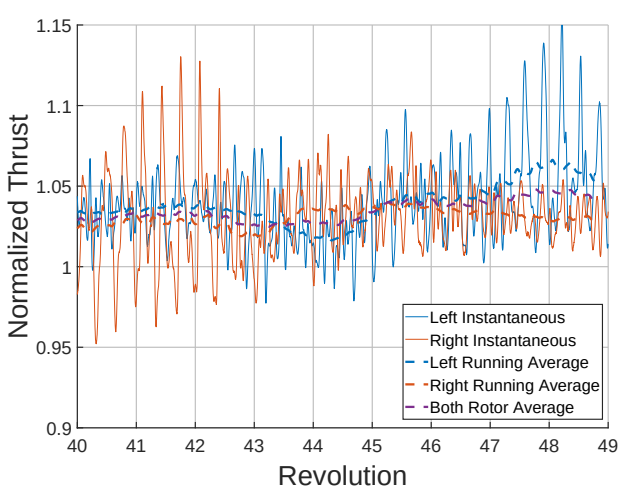

Figure 18. Thrust history of each side-by-side rotor at H/D = 0.5 and 2.5R hub-hub separation, including instantaneous, single rotor rev-averaged thrust and both rotor rev-averaged thrust normalized by isolated OGE thrust

Figure 16 shows the difference in sectional thrust coefficient between two H/D = 0.5 IGE rotors with 2.5R hub-hub separation and an OGE single rotor (IGE minus OGE), averaged over three revolutions. Like the other H/D = 0.5 case discussed, moderate thrust increment is observed inboard. Thrust deficit is observed near the tips, and is significantly stronger between the rotors. Again, strong turbulence in the mixing region between rotors leads to thrust losses when blades pass through.

Figure 17 shows a slice colored by vorticity magnitude cutting through both side-by-side rotor hubs at H/D = 0.5 with 2.5R hub-hub separation. The tip paths of both rotors is annotated in cyan. The mixing between the rotors for this case occupies a smaller area than that observed in Fig. 14. The turbulence remains relatively stationary in the inter-rotor region, and does not fountain over the disk plane as in Fig. 14. Whereas the 3.0R separation case saw strong vorticity magnitude fountaining onto inboard portions of the disks, only the blade tips encounter the turbulent mixing region at 2.5R separation. Additionally, with blade tips only separated by 0.5R, the turbulent mixing does not have room to move laterally closer to one rotor over the other.

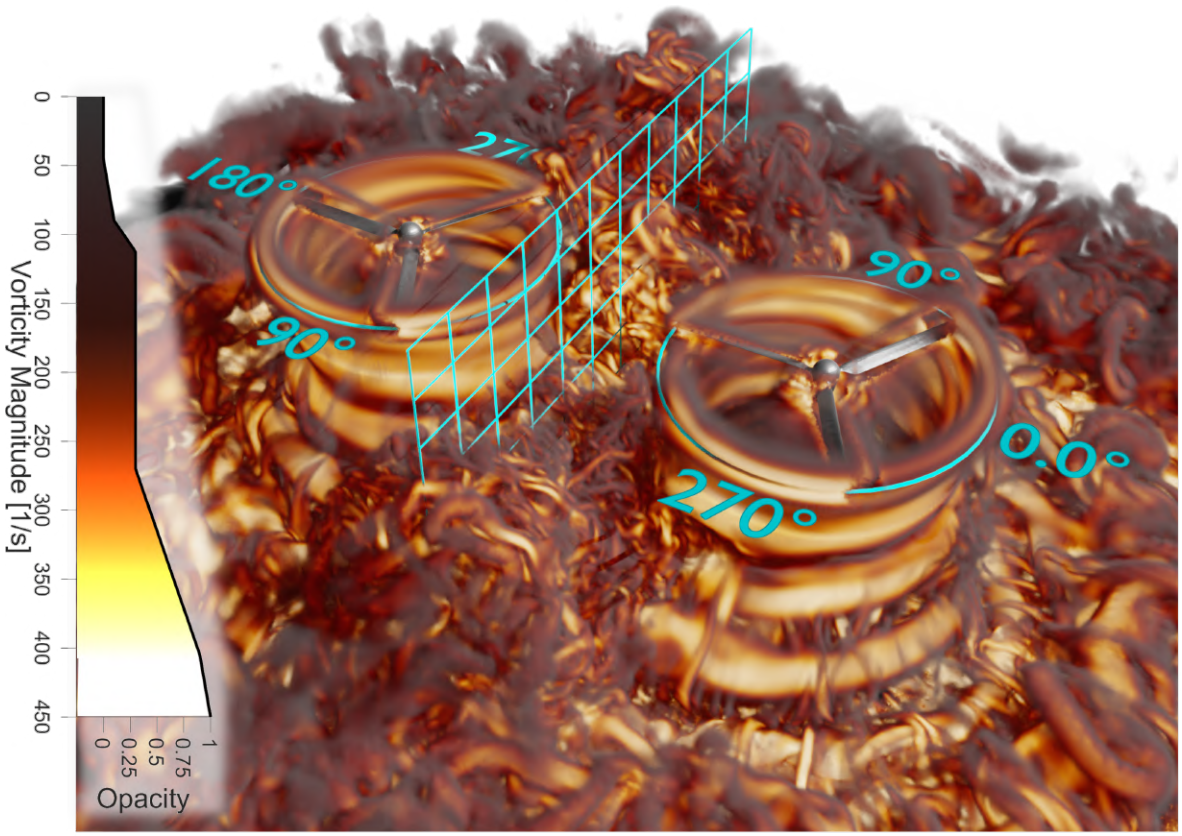

Figure 19. Direct volume rendering of H/D = 1, 3.0R separation side-by-side rotors with opacity and color dictated by vorticity magnitude

With a majority of the thrust deficit on only one side of the disk (as seen in Fig. 16), impulsive loading is induced. Figure 18 shows the thrust history for each side-by-side rotor at H/D = 0.5 and 2.5R separation normalized by isolated OGE rotor thrust. Single rotor running rev-averaged thrust over time as well as both rotor running rev-averaged thrust are also plotted. Vibratory loading for these rotors is substantial, with instantaneous thrust oscillating peak-to-peak up to 16% from the running average. Impulsive loads are seen three times per revolution for each rotor, corresponding to blade passage through the highly turbulent flow between the rotors. Vibratory loading at 3/Rev is stronger at 2.5R separation than 3.0R separation. This could be attributed to blade tips at 2.5R encountering a concentrated mixing region, whereas the blade tips and inboard regions at 3.0R separation encounter more dispersed vortical mixing.

Average thrust for the 2.5R separation rotors is not steady from revolution to revolution either. Single revolution average thrust for the left rotor changes by almost 5% over the period simulated, and the right rotor by 2%. The average thrust discrepancy between rotors is less than that observed when separation was 3.0R. With less substantial thrust losses between the rotors, thrust increment inboard leads to a net thrust improvement compared to OGE. Averaging over three revolutions at 1° timesteps, the side-by-side rotors at H/D = 0.5 with 2.5R spacing produce 4.3% more thrust than a single rotor OGE.

Side by Side H/D = 1

Side-by-side rotors are also simulated higher from the ground, at H/D = 1. Figure 19 shows direct volume rendering of vorticity magnitude for side-by-side rotors at H/D = 1 and 3.0R hub-hub separation. The cyan grid between the rotors extends 1R above the rotor plane, and to the ground (2R) below. From $\psi = 270°$ to 90° (through 0°), the right rotor wake convects downwards until it impacts the ground and spreads radially. Between the rotors, the wake still convects downwards until it reaches close to the ground. Instead of moving radially along the ground however, the wake of each rotor impinges on the other, and mixes near the ground plane. The wake mixing remains primarily within one rotor radii of the ground plane, and does not reach the rotor plane.

Figure 20 plots sectional thrust coefficient difference between an isolated OGE rotor and side-by-side rotors at H/D = 1 and 3.0R separation. No thrust increment is observed inboard as the rotors are too high off the ground to encounter significant fountaining over the inboard sections. Like with the isolated IGE rotor at H/D = 1, moderate thrust deficit is observed near the blade tips. Between the rotors, additional thrust deficit is observed.

Side-by-side rotors at H/D = 1 produce lesser vibratory loading than at H/D = 0.5. Figure 21 plots the thrust history of each side-by-side rotor at 1.0 H/D with 3.0R hub-hub separation normalized by isolated OGE thrust. Running aver-

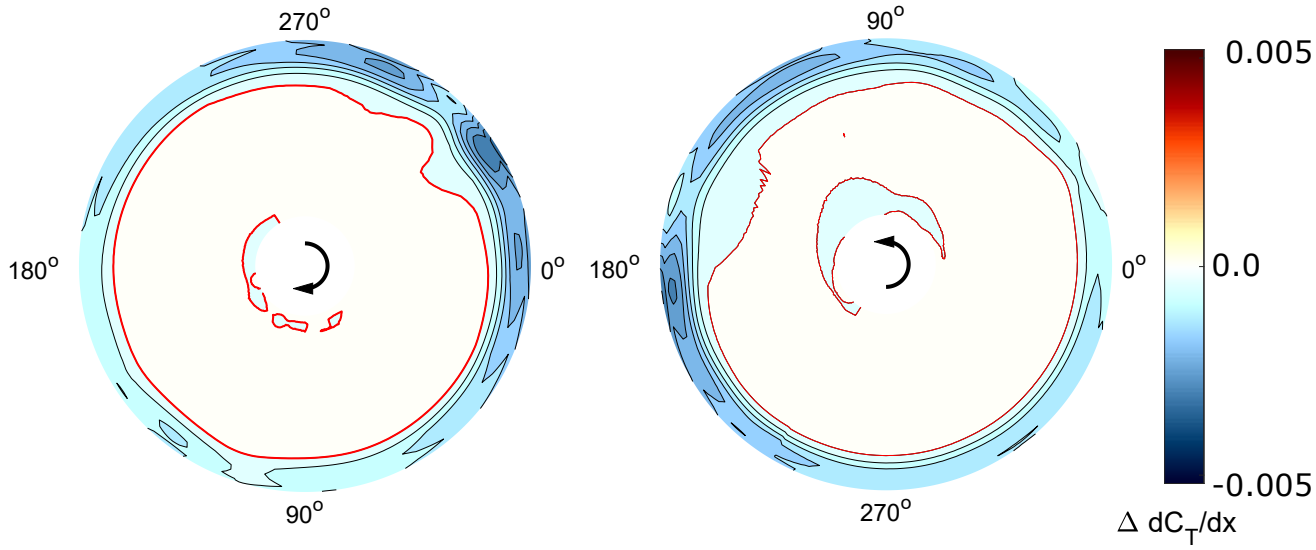

Figure 20. Three revolution average sectional thrust coefficient difference between side-by-side H/D = 1 rotors with 3.0R spacing and a single out of ground effect rotor (IGE minus OGE)

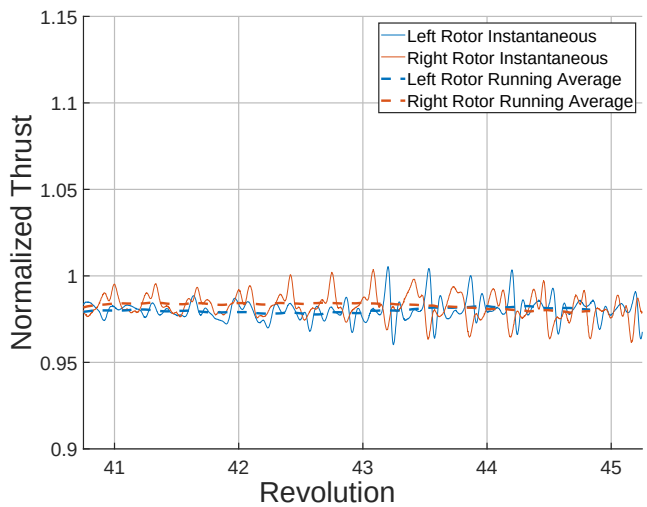

Figure 21. Thrust history of each side-by-side rotor at H/D = 1 and 3.0R hub-hub separation, including instantaneous, single rotor rev-averaged thrust and both rotor rev-averaged thrust normalized by isolated OGE thrust

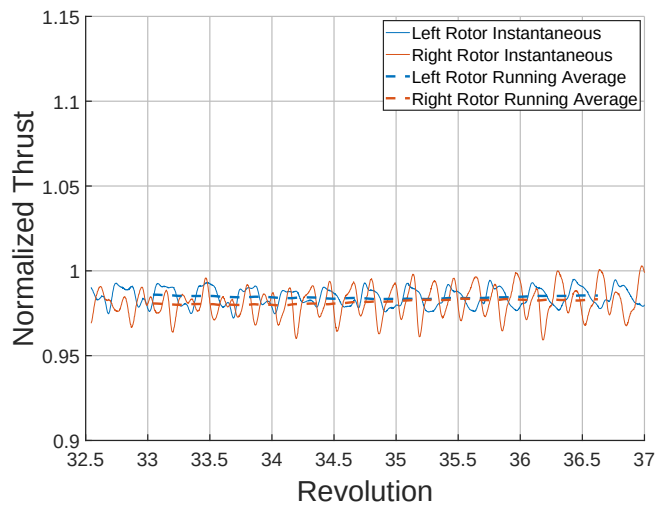

Figure 22. Thrust history of each side-by-side rotor at H/D = 1 and 2.5R hub-hub separation, including instantaneous, single rotor rev-averaged thrust and both rotor rev-averaged thrust normalized by isolated OGE thrust

age thrust over one revolution is also plotted for each rotor. Peak to peak loading up to 4% mean thrust is observed, significantly less than at H/D = 0.5. Reduced vibratory loading is attributed to the turbulent mixing region between the rotors staying below the rotor plane. Mean thrust for rotors at H/D = 1 is relatively constant, and does not vary from revolution to revolution like rotors at H/D = 0.5. Mean thrust for these rotors is consistently about 2.8% less than an isolated OGE rotor due to the lift deficit at the tip observed in Fig. 20.

Side-by-side rotors at H/D = 1 with 2.5R hub-hub separation are also simulated. Figure 23 shows direct volume rendering of vorticity magnitude for side-by-side rotors at H/D = 1 and 2.5R hub-hub separation. Like the other IGE rotors, the wake from $\psi = 270°$ to 90° through 0° convects radially after impacting the ground. Between the rotors, the wakes collide approximately 1R above the ground. With less space for mixing to develop, the turbulent region between the rotors does not extend as high as that observed at H/D = 1 and 3R separation.

Thrust losses for side-by-side rotors at H/D = 1 and 2.5R hub-hub separation are similar in distribution and magnitude to those observed at 3.0R hub-hub separation (Figs. 24, 22). No thrust increment is observed inboard, and lower thrust deficit is seen between the rotors than the H/D = 0.5 case. Vibratory loading has peak-to-peak values up to 4% of mean thrust. Mean thrust does not show much variation, but is 2.7% less than an isolated OGE rotor. Mean thrust for each rotor is steady with time.

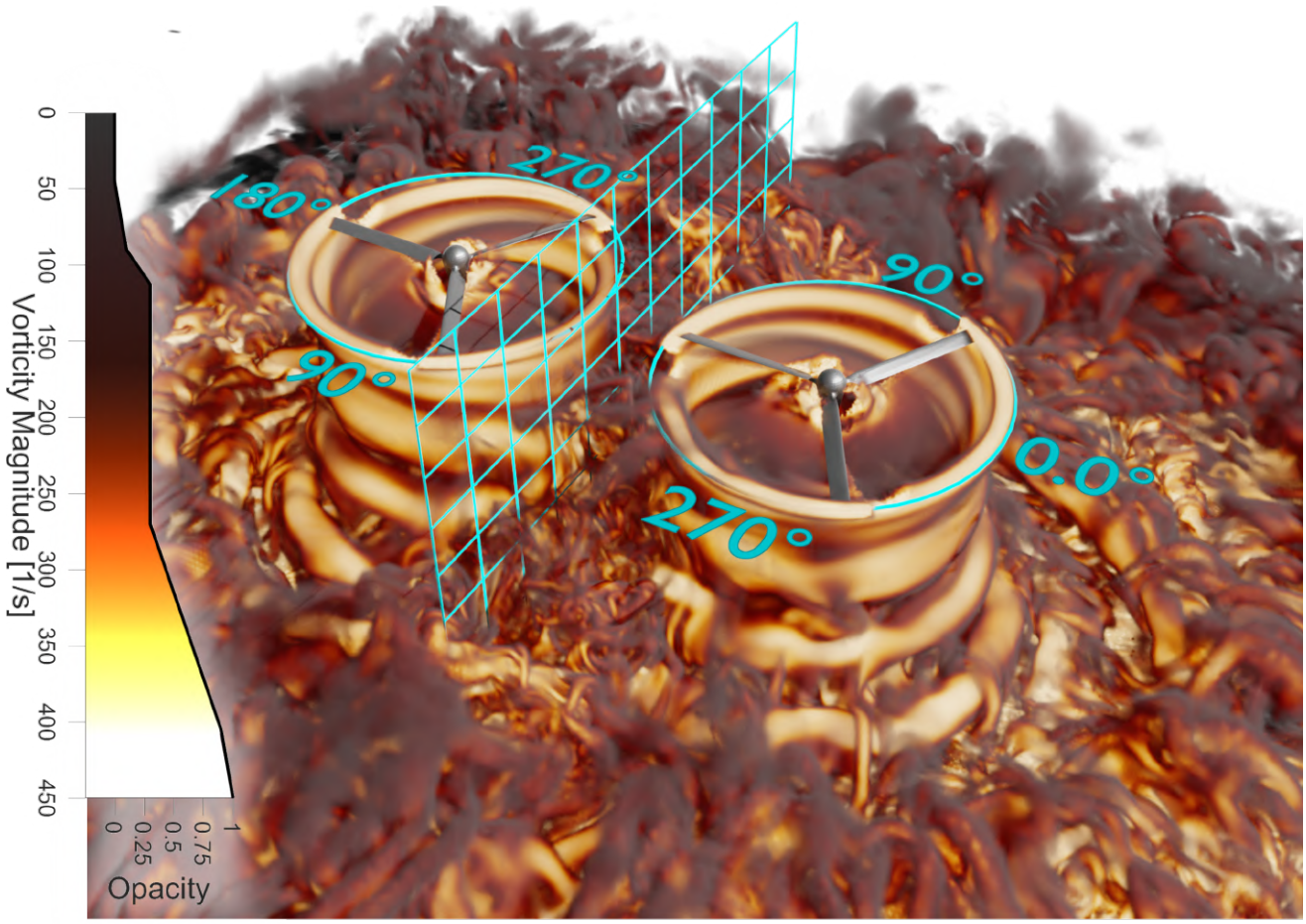

Figure 23. Direct volume rendering of H/D = 1, 2.5R separation side-by-side rotors with opacity and color dictated by vorticity magnitude

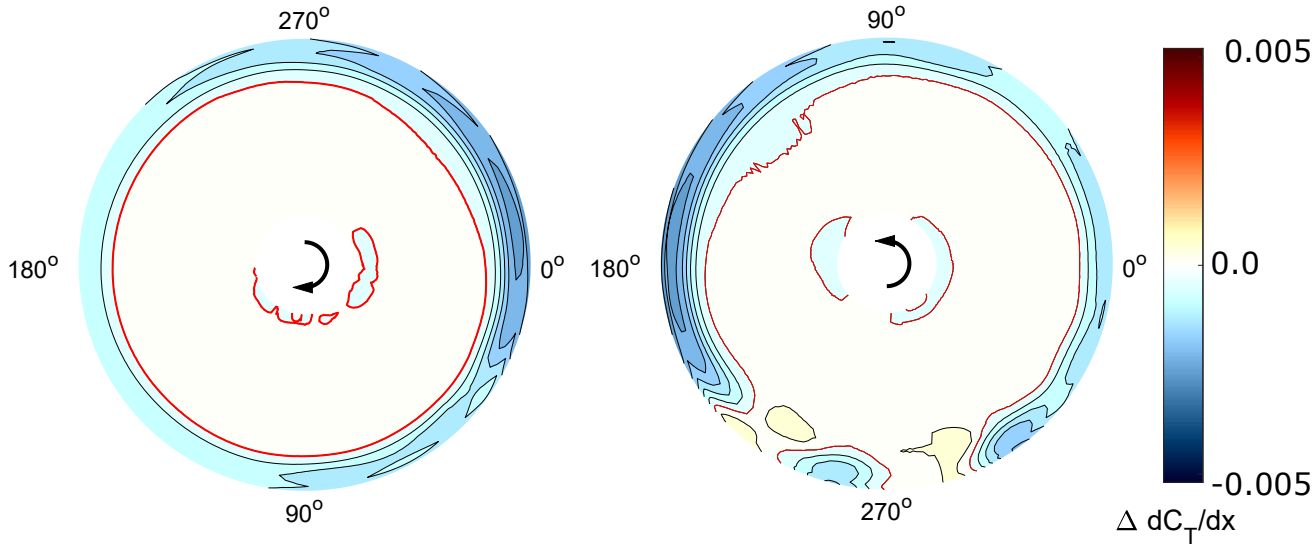

Figure 24. Three revolution average sectional thrust coefficient difference between side-by-side H/D = 1 rotors with 2.5R spacing and a single out of ground effect rotor (IGE minus OGE)

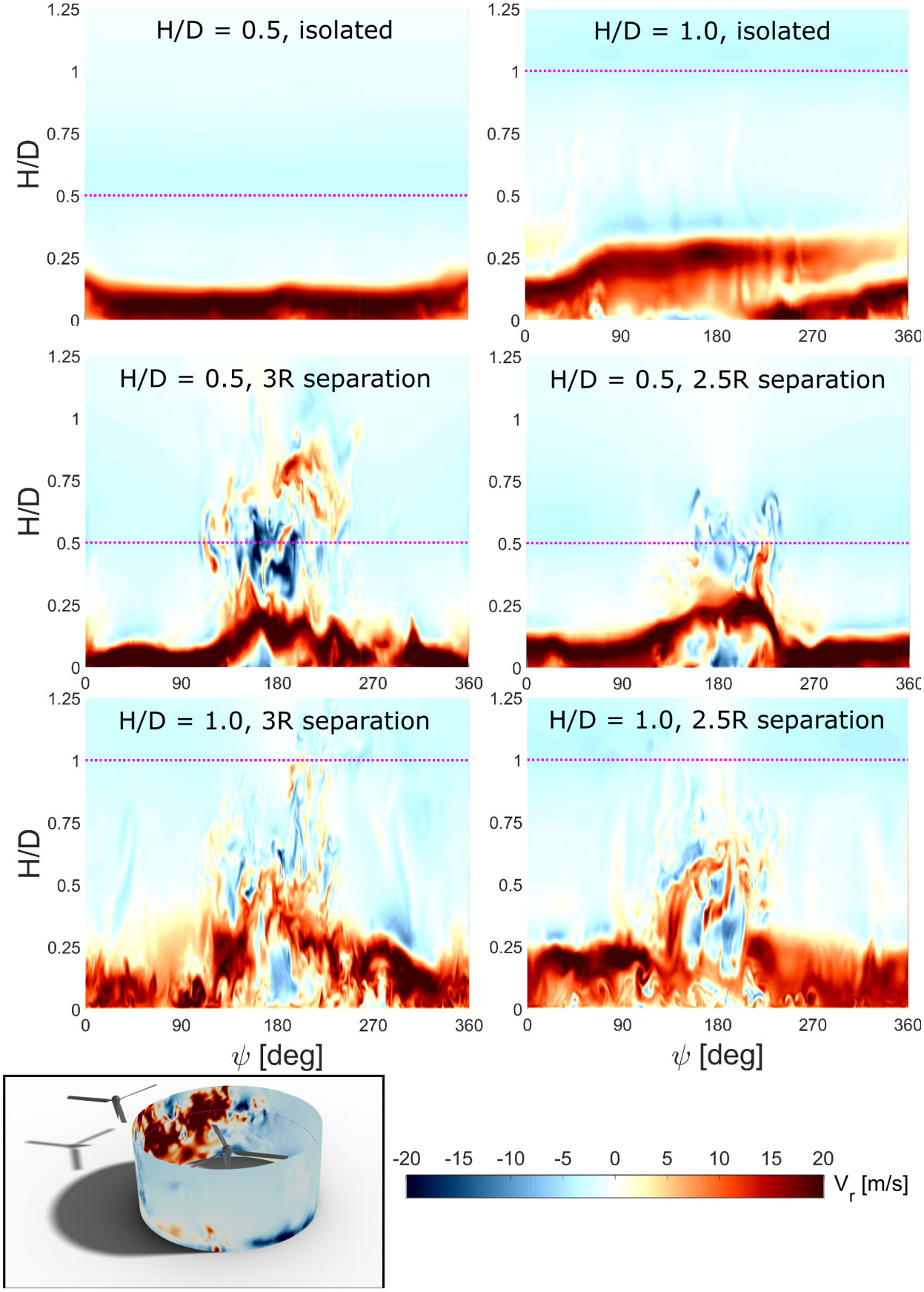

Figure 25. Unwrapped cylinders colored by radial velocity for IGE rotor cases described in Fig. 1

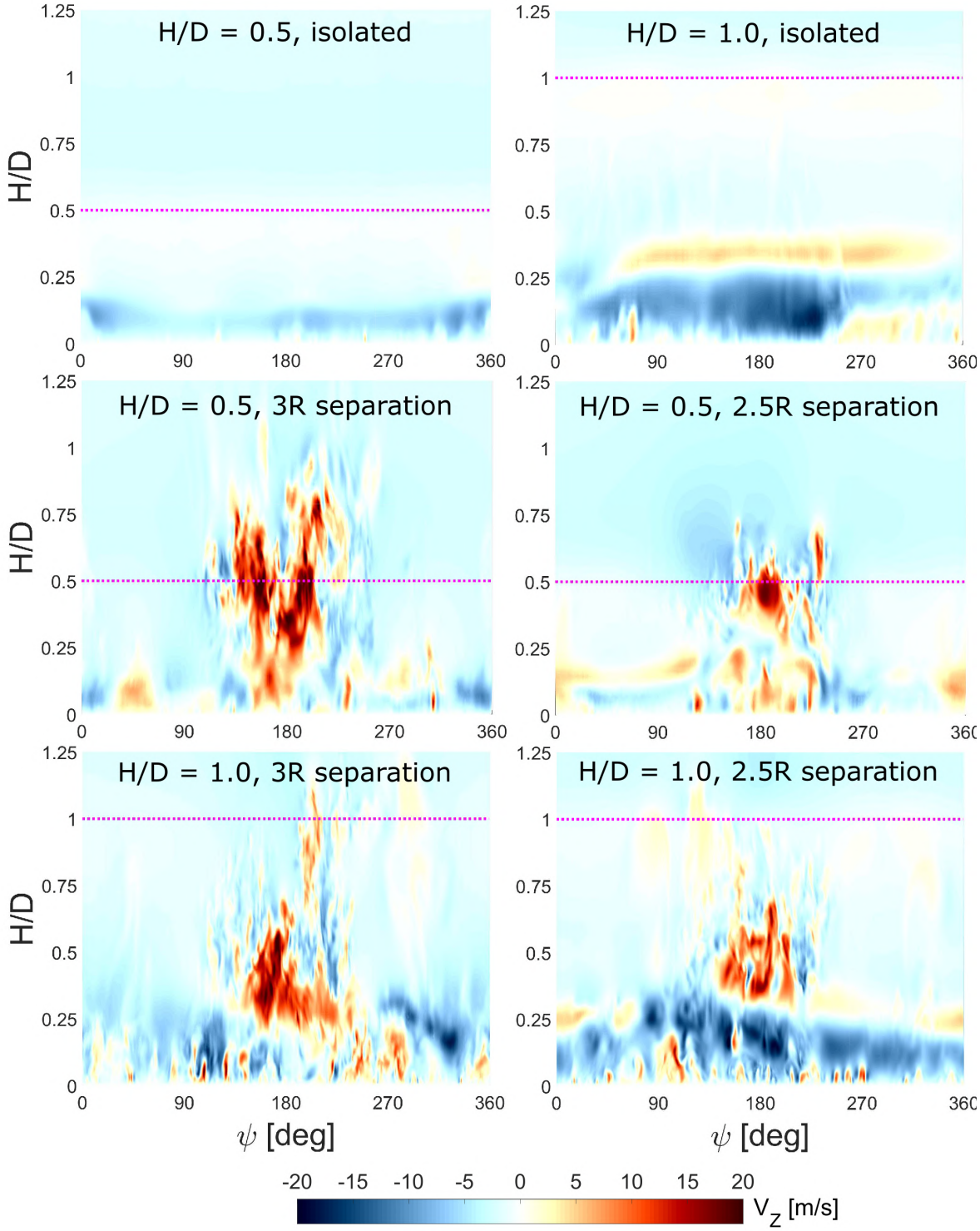

Figure 26. Unwrapped cylinders colored by vertical velocity for IGE rotor cases described in Fig. 1

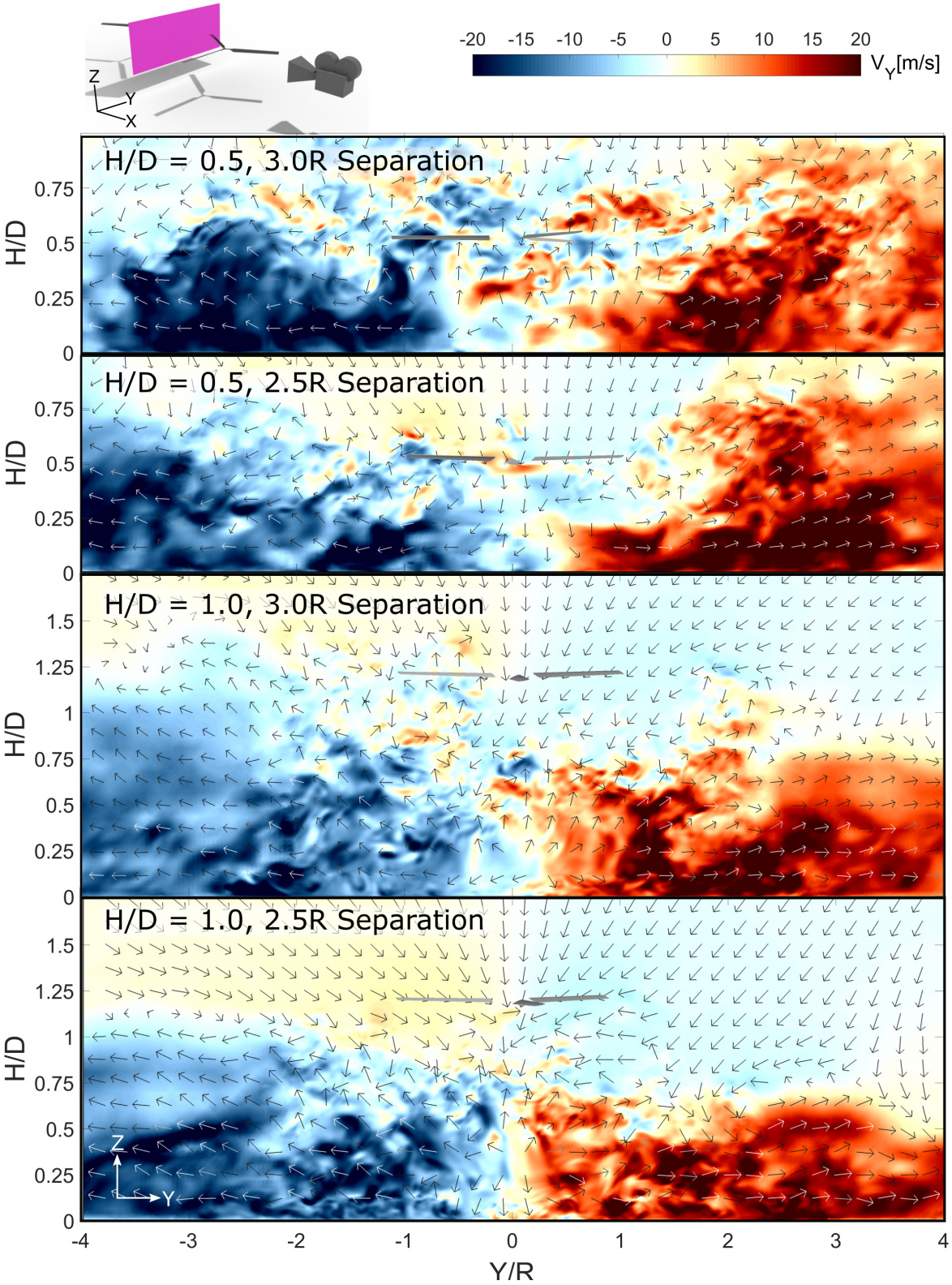

Figure 27. Slice cutting longitudinally between side-by-side rotors colored by longitudinal velocity

OUTWASH COMPARISON

When the wake of an isolated rotor IGE impacts the ground, it is able to freely convect radially away from the rotor. As the wake skirts along the ground, it induces a net radial velocity. This can be seen for isolated rotors at H/D = 0.5 and H/D = 1 in Fig. 25. This figure plots an unwrapped cylinder extending from the ground plane to a height of 1.25D (2.5R) around an isolated rotor or the right rotor of the two rotor systems considered in this study. The colors indicate the magnitude of the radial velocity. The cylinder radius extends 1.25R for the isolated rotors, and to the middle (symmetry plane) of the side-by-side rotors. Thus, the cylinder radius is 1.25R or 1.5R depending on whether the hub-to-hub separation is 2.5R or 3R respectively for the two rotor cases. The cylinder (diagramed in the bottom-left) is unwrapped to form a 2D plane. A magenta line is plotted along the projection of the tip path plane. For the isolated rotors, a skirt of radial velocity exceeding 20 m/s is observed within 0.25D of the ground.

When a second, nearby rotor is introduced (in the side-by-side configuration), the wakes of each rotor interfere with each other. Outside the rotors, ($\psi = 270^\circ - 0^\circ - 90^\circ$), the same radial velocity is seen as with the isolated rotors. Between the rotors, however, wake mixing leads to radial velocity being bidirectional (into or out of the cylinder). The mixing regions for 3.0R separation cases tend to occupy a larger range of azimuths than 2.5R separation cases. Rotors at H/D = 1 operate primarily above the mixing region.

Figure 26 shows the same unwrapped cylinders as Fig. 25, but colored by vertical velocity. The downwards vertical velocity observed for the isolated cases near the ground is the result of a tip vortex outside the cylinder locally inducing downwash at the radial location and time instant plotted. For side-by-side rotor cases, only moderate vertical velocity is induced away from the other rotor ($\psi = 270^\circ - 0^\circ - 90^\circ$). In the mixing region between the rotors ($\psi = 90^\circ - 180^\circ - 270^\circ$), predominantly upwash is induced as the rotor wakes collide and fountain. For side-by-side rotors at H/D = 1 and 2.5R separation, the wakes at $\psi = 180^\circ$ are found to collide 0.25D above the ground plane, inducing upwash above, and downwash below.

In the inter-rotor region, while the colliding wakes result in part of the flow moving upward (vertical fountain), a substantial part of the flow leaves that region laterally (sideways, in the $\pm$Y direction). Figure 27 shows slices positioned equally between side-by-side rotors colored by Y-velocity. Blue indicates velocity moving towards the right rotor's $\psi = 270^\circ$ direction, and red towards the right rotor's $\psi = 90^\circ$ direction. For all side-by-side cases, the flow between the rotors cannot move radially as when they were are isolation, and instead must move laterally to escape the system. Lateral outwash for all cases is as strong (exceeding 20 m/s) as the radial outwash for the isolated rotors, and extends higher vertically above the ground plane. While the skirt of radial velocity for an isolated rotor only extended 0.25D above the ground, lateral flow for H/D = 0.5 is observed to propogate up to 1D above the ground plane. The vertical extents of lateral flow for H/D = 0.5 cases is vertically higher than that observed for H/D = 1, where lateral outwash only extends 0.75D above the ground plane.

INTEGRATED LOAD COMPARISON

Interactional aerodynamics has been seen to influence the thrust performance of side-by-side rotors in ground effect. Figure 28 compares time averaged integrated thrust for all six IGE cases discussed. Thrust values are presented relative to the thrust generated by an isolated OGE rotor. An isolated rotor at H/D = 0.5 provides the greatest thrust improvement, producing 6.4% more thrust than if out of ground effect. If positioned higher from the ground, at H/D =1.0, the isolated rotor no longer receives thrust increment from fountaining through the hub, and does not see a thrust improvement. Despite receiving thrust increment inboard, side-by-side rotors at H/D = 0.5 with 3.0R hub-hub spacing produce less thrust than an isolated OGE rotor. Thrust deficits in the region of the blade tips, especially in the region between the rotors where there is turbulent mixing negates any inboard thrust increment, leading to a net loss in thrust. Side-by-side rotors IGE at H/D = 0.5 and with relatively smaller 2.5R hub-hub spacing provide some net increment in steady thrust, producing 4.5% more thrust than an isolated OGE rotor. However, the increase is less than that observed for an isolated rotor at the same height above the ground due to the blades encountering turbulent mixing between the rotors. Side-by-side rotors at H/D = 1 do not see any lift increment from fountianing through the hub region, and show a small (2%) thrust deficit due to lift loss between the rotors.

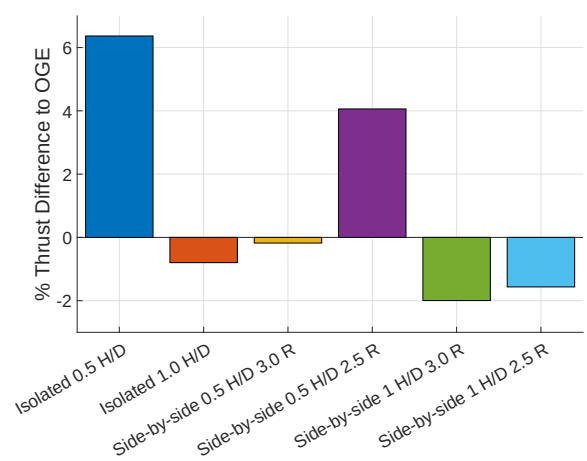

Figure 28. Relative thrust difference between six IGE rotor cases and an isolated OGE rotor (IGE minus OGE)

CONCLUSIONS

This study investigates the interactional aerodynamics of side-by-side rotors in ground effect. The computational fluid dynamics code AcuSolve, with Detached Eddy Simulation, was used to simulate the aerodynamics of the system. The sliding

mesh method was used to simulate blade motion by interfacing two rotating volumes (one for each rotor) within a non-rotating volume. Every simulation was performed with 5.5 ft diameter, 3 bladed rotors with uniform planform and linearly twisted blades spinning at 1600 RPM, corresponding to a 5 lb/ft^2 target disk loading. In all, seven cases were simulated: isolated out of ground effect, isolated in ground effect at H/D = 0.5 and H/D = 1, side-by-side rotors at H/D = 0.5 with 3.0R and 2.5R hub-hub separation, and side-by-side rotors at H/D = 1 with 3.0R and 2.5R separation. The performance of isolated and side-by-side rotors in ground effect were compared to the performance of an isolated out of ground effect rotor. Through these simulations, the following observations were made.

1. Between side-by-side rotors in ground effect, the wakes of each rotor collide, inducing turbulent mixing.

2. Turbulent mixing between side-by-side rotors induce thrust penalties over the outboard sections of the blades as they pass through the inter-rotor region.

3. Side-by-side rotors at 3.0R separation provide more space for vortical superstructures to develop between the rotors than when at 2.5R separation.

4. Turbulence between the rotors at 3.0R separation fountains up, over the disk plane, leading to stronger thrust deficits than at 2.5R separation.

5. The space between rotors at 3.0R separation allows for vortical structures to move side-to-side over multiple revolutions. As pockets of strong turbulence move closer to one of the rotors, its thrust average reduces, while the peak-to-peak variation increases significantly (up to 10%).

6. The simulated rotors at H/D = 1 do not observe thrust increment inboard due to fountaining through the hub (unlike H/D = 0.5 rotors), and display significantly lower vibratory loading than rotors at H/D = 0.5.

7. The colliding wakes of the two rotors causes the flow to fountain upward, as well as to exit the inter-rotor region laterally (in a direction perpendicular to a plane containing the two rotor hubs).

REFERENCES

1. M. Misiorowski, F. Gandhi, and A. A. Oberai, "Computational study on rotor interactional effects for a quadcopter in edgewise flight," *AIAA Journal*, vol. 57, no. 12, pp. 5309–5319, 2019.

2. M. Misiorowski, F. Gandhi, and P. Anusonti-Inthra, "Computational analysis of rotor-blown-wing for electric rotorcraft applications," *AIAA Journal*, vol. 58, no. 7, pp. 2921–2932, 2020.

3. R. Healy, M. Misiorowski, and F. Gandhi, "A systematic CFD-based examination of rotor-rotor separation effects on interactional aerodynamics for large eVTOL aircraft," in *Proceedings of the 75th Annual Forum*, (Philadelphia), VFS International, May 2019.

4. R. Healy, F. Gandhi, M. Mistry, and M. Duffy, "A computational investigation of multi-rotor interactional aerodynamics with hub lateral and longitudinal canting," in *Proceedings of the 76th Annual Forum*, (Virtual), The Vertical Flight Society, October 2020.

5. P. V. Diaz and S. Yoon, "High-fidelity computational aerodynamics of multi-rotor unmanned aerial vehicles," in *2018 AIAA Aerospace Sciences Meeting*.

6. S. Yoon, T. H. Pulliam, and N. M. Chaderjian, "Simulations of XV-15 rotor flows in hover using OVERFLOW," in *AHS 5th Aeromechanics Specialists' Conference, San Francisco, CA, USA*, Jan 2014.

7. S. Yoon, H. C. Lee, and T. H. Pulliam, "Computational analysis of multi-rotor flows," in *AIAA 54th Aerospace Sciences Meeting, San Diego, CA, USA*, Jan. 2016.

8. S. Yoon, P. V. Diaz, D. D. Boyd Jr., W. M. Chan, and C. R. Theodore, "Computational aerodynamic modeling of small quadcopter vehicles," in *Proceedings of the 73rd Annual Forum*, (Fort Worth), AHS International, May 2017.

9. E. A. Fradenburgh, "The helicopter and the ground effect machine," *Journal of the American Helicopter Society*, vol. 5, pp. 24–33, Oct. 1960.

10. A. Wadcock, L. Ewing, E. Solis, M. Potsdam, and G. Rajagopalan, "Rotorcraft downwash flow field study to understand the aerodynamics of helicopter brownout," in *Proceedings of the AHS Southwest Region Technical Specialists' Meeting*, p. 28, 10 2008.

11. B. Kutz, T. Grossmann, M. Keßler, and E. Krämer, "Experimental and numerical examination of a helicopter hovering in ground effect," in *CEAS Aeronautical Journal*, vol. 4, pp. 397–408, 09 2013.

12. V. K. Lakshminarayan, T. S. Kalra, and J. D. Baeder, "Detailed computational investigation of a hovering microscale rotor in ground effect," *AIAA Journal*, vol. 51, no. 4, pp. 893–909, 2013.

13. T. Lee, J. Leishman, and M. Ramasamy, "Fluid dynamics of interacting blade tip vortices with a ground plane," *Journal of the American Helicopter Society*, vol. 55, p. 022005, 04 2010.

14. A. Zanotti, G. Gibertini, D. Grassi, and D. Zagaglia, "Experimental investigation on the aerodynamic interaction between a helicopter and ground obstacles," *Proceedings of the Institution of Mechanical Engineers Part G Journal of Aerospace Engineering*, vol. 229, pp. 1395–1406, 05 2015.

15. J. Tan, Y. Sun, T. Zhou, G. N. Barakos, and R. B. Green, "Simulation of the aerodynamic interaction between rotor and ground obstacle using vortex method," in *Proceedings of the 74th Annual Forum*, (Phoenix), AHS International, May 2018.

16. R. Boisard, "Aerodynamic investigation of a helicopter rotor hovering in the vicinity of a building," in *Proceedings of the 74th Annual Forum*, (Phoenix), AHS International, May 2018.

17. V. Gupta and J. D. Baeder, "Quad tiltrotor aerodynamics in ground effect," in *Proceedings of the 58th Annual AHS Forum*, (Montreal), AHS International, June 2002.

18. S. Miesner, M. Ke, E. Krämer, and U. Schäferlein, "Investigation of near ground effects in hover flight for the multi-rotor aircraft Volocopter-2X," in *Proceedings of the 76th Annual Forum*, (Virtual), The Vertical Flight Society, October 2020.

19. N. S. Hariharan, R. P. Narducci, E. Reed, and A. Egolf, "AIAA standardized hover simulation: Hover performance prediction status and outstanding issues," in *55th AIAA Aerospace Sciences Meeting*, 2017.

20. J. Abras, R. P. Narducci, and N. S. Hariharan, "Impact of high-fidelity simulation variations on wake breakdown of a rotor in hover," in *AIAA Scitech 2020 Forum*.

21. R. Niemiec and F. Gandhi, "Development and validation of the Rensselaer Multicopter Analysis Code (RMAC): A physics-based low-fidelity modeling tool," in *75th Annual Forum of the Vertical FLight Society*, (Philadelphia), 2019.

22. I. ACUSIM Software, "Acusolve validation - NACA 0012 airfoil," tech. rep., http://altairhyperworks.com/ResourceLibrary.aspx?category=Case2010, 2010.

23. D. Corson, R. Jaiman, and F. Shakib, "Industrial application of RANS modelling: capabilities and needs," *International Journal of Computational Fluid Dynamics*, vol. 23, no. 4, pp. 337–347, 2009.

24. M. Misiorowski, F. Gandhi, and A. A. Oberai, "Computational study on rotor interactional effects for a quadcopter in edgewise flight," *AIAA Journal*, 2019. https://doi.org/10.2514/1.J058369.

25. Altair Engineering Inc., *Modeling of Turbulence - Near-Wall Modeling*. acusolve/training_manual/near_wall_modeling_r, 2019.

26. Y. Bazilevs, C. Michler, V. Calo, and T. Hughes, "Weak dirichlet boundary conditions for wall-bounded turbulent flows," *Computer Methods in Applied Mechanics and Engineering*, vol. 196, no. 49, pp. 4853 – 4862, 2007.

27. K. E. Jansen, C. H. Whiting, and G. M. Hulbert, "A generalized- method for integrating the filtered Navier–Stokes equations with a stabilized finite element method," *Computer Methods in Applied Mechanics and Engineering*, vol. 190, no. 3, pp. 305 – 319, 2000.

28. A. N. Brooks and T. J.R. Hughes, "Streamline upwind/Petrov-Galerkin formulations for convection dominated flows with particular emphasis on the incompressible Navier-Stokes equations," *Computer Methods in Applied Mechanics and Engineering*, vol. 32, pp. 199–259, 09 1982.